THE PENNSYLVANIA STATE UNIVERSITY
SCHREYER HONORS COLLEGE

DEPARTMENT OF CIVIL ENGINEERING

A Comparison Study and Optimization of Input Parameters for Thermal Conductivity Testing of Concrete

NAUFAL MURTADZA
Semester of Graduation SPRING 2022

A thesis
submitted in partial fulfillment
of the requirements
for a baccalaureate degree
in Civil Engineering
with honors in Civil Engineering

Reviewed and approved* by the following:

Grady F. Mathews, IV
Assistant Professor of Civil Engineering
Thesis Supervisor

David S. Witwer
Professor of American Studies
Honors Adviser

* Electronic approvals are on file.

ABSTRACT

Past studies on thermal conductivity of concrete use these three types of methods which include the two linear parallel probe (TLPP), transient plane source (TPS), and hot guarded plate (HGP). The test method requires the test samples to be fixed between hot and cold plates so a constant heat stream can flow over the test samples. This project uses the Transient Plane Source (TPS) method to measure thermal conductivity by sandwiching a singular spiraling flat sensor and probe between two concrete disks. The electric current passes through the probe to increase the heat, and the sensor will measure the thermal conductivity. But factors that are not mentioned in the ACI 122R Guide to Thermal Properties of Concrete and Masonry systems, such as the sensor location and measurement time, may affect the sample's thermal conductivity value since it is related to the thermal diffusivity value. Furthermore, with the increase in demand for a more sustainable concrete, foamed glass aggregate (FGA) is added to the concrete mix for the project as it was previously observed to have insulation capability in concrete. However, further study about FGA is needed to understand how it affects the concrete's expansion. Only a few past studies determine how significant the sensor location, measurement time, and FGA influence the result. Hence, further research is needed to optimize the input parameters of thermal conductivity testing concrete to get the most accurate results.

TABLE OF CONTENTS

LIST OF FIGURES

LIST OF TABLES

LIST OF EQUATIONS

ACKNOWLEDGEMENTS

Firstly, I would like to express my gratitude to Dr. Grady Mathews for his fantastic support and guidance in the laboratory and the classrooms and throughout my development as an undergraduate student studying civil engineering. He always provides me with the opportunity to grow out of myself and connect to outstanding civil engineering faculties and students throughout Penn State and beyond.

Secondly, I would like to thank David Boyd for ensuring I have everything I need in the civil engineering materials laboratory while making sure we always think about our safety. He always holds the source of wisdom in the laboratory in life due to his vast experience.

Third, I would like to thank Dr. Farshad Rajabipour and Ph.D. candidate Jafari Khashayar from Penn State, University Park, for allowing me to briefly experience graduate student research life at Penn State while supporting me in every way to experiment and learn the Alkali-Silica Reaction test at one of their state-of-the-art laboratories.

Fourth, I would like to thank Dr. Rajarajan Subramanian for being my civil engineering advisor throughout my undergraduate years. He helped me with the first step in doing research during my sophomore year and guided me every semester in getting courses for my degree.

Finally, I would like to thank Penn State, Penn State MC-REU, the Schreyer Honors College, and the Drawdown project for allowing me this opportunity and generously giving me multiple research grants to study more about my passion for researching sustainable concrete.

Chapter 1

Introduction

In temperate regions of the world, it takes a lot of energy to maintain a comfortable temperature and environment for humans to do their daily activities in households, commercial, and office spaces. In the winter, buildings need to be heated, and in the summer, buildings need to be cooled. These actions are done by using central heating or air conditioning system that consumes electricity. Suppose the facilities or spaces are built with poorly insulated walls. In that case, the rooms inside will lose the temperature control from the centralized heating/cooling system and try to follow the temperature outside. This situation will push the system harder hence increasing electricity use. This high amount of electricity used in buildings will create a negative environmental impact as many electric power plants still rely on fossil fuels to produce electricity.

A demand for a more energy-efficient buildings has been seen throughout the world. As a result, the United States and European countries have generally adopted building codes to ensure energy-conservation standards in facilities (Sargam et al. 2020; Yun et al. 2013). One action that can be done is to maintain the low thermal conductivity of building walls that commonly consist of concrete and masonry. The reduction of heat loss in building walls through modification in concrete helps decrease energy consumption, increase insulation, and improve sustainability (Sengul et al. 2011).

Concrete typically consists of different materials, including Ordinary Portland Cement (OPC), coarse aggregates, fine aggregates, admixtures, and water. It is hard to predict the

thermal properties of concrete because there are differences in the thermal expansion of material components within concrete (Nguyen et al. 2019). Hence, efforts to reduce thermal conductivity have been made by modifying the contents of the concrete itself. The thermal conductivity of concrete is reduced by incorporating perlite (Demirboğa and Gül 2003) and lightweight aggregates (del Coz Díaz et al. 2007).

One typical example of lightweight aggregates used in the industry is foamed glass aggregates (FGA). FGA is manufactured by processing mixed container glass into powder and applying a foaming agent at a high temperature. FGA is known to be several times lighter compared to the traditional limestone coarse aggregate that is used with cementitious materials to create concrete. It also has the function of providing increased insulation for concrete because of its porous structure. Even though FGA has its benefits, there are limited numbers of experimental work being done to investigate the properties of FGA, especially its application in concrete. Besides the porosity of the aggregate, the thermal conductivity is also affected by the cement dosage, slump, and density of concrete (Uysal et al. 2004).

Primarily there are three standard methods of measuring the thermal conductivity of a material: Hot Guarded Plate (GHP), Two Linear Parallel Probe (TWLPP), and Transient Plane Source (TPS). Even though methods have their advantages, they use the same basic concept of emitting heat using a probe to emit heat through the material and use a sensor at the other end to record the thermal conductivity. For the measurements to run, input parameters need to be determined to get the correct recording of the thermal conductivity. Input parameters, measuring time, and probing depth significantly impact concrete thermal conductivity. A limited number of studies discuss how the inclusion of recycled aggregates affects the insulation of concrete and its

measurement since the mixture is heterogeneous. The heterogeneous nature of the concrete's surface poses a challenge in determining its thermal conductivity because each component has different values. The thermal conductivity of the cementitious materials will be different from the more porous aero aggregate. Hence further study is needed to find the most sustainable and suitable material in ensuring proper insulation for buildings.

Chapter 2

Literature Review

Methods of Measuring Thermal Conductivity

Concrete is a highly heterogeneous material, which means that it consists of different materials such as aggregates and cement. The main challenge of measuring a heterogeneous material is that its content has a different thermal conductivity. Over the recent decades, several methods and standards of thermal conductivity measurements for concrete have been developed to overcome this challenge. Such methods are divided into two categories: steady and transient methods (Sargam et al. 2020). Commonly, past studies on thermal conductivity of concrete use these three types of methods which includes the two linear parallel probe (TLPP), plane heat source (PHS) and hot guarded plate (HGP) (Asadi et al. 2018).

Hot Guarded Plate (HGP)

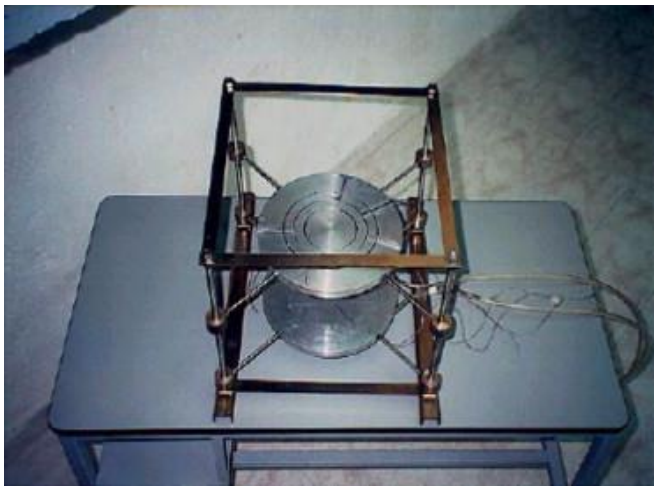

Figure 1. Guarded hot plate apparatus for measuring the thermal conductivity of insulating solid materials (Xamán et al. 2009)

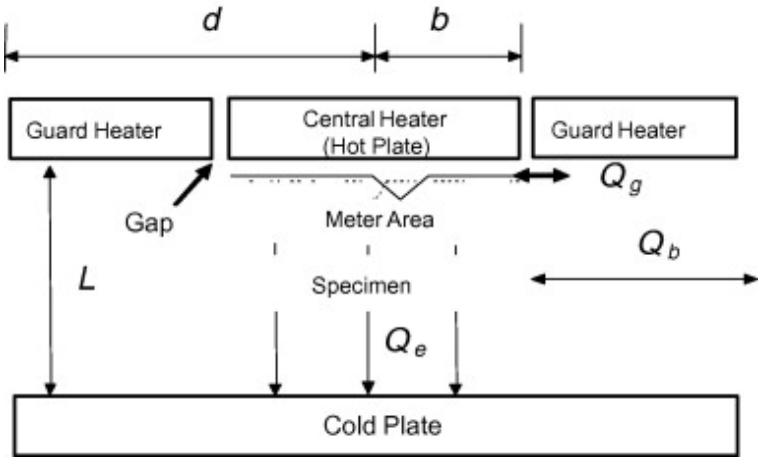

Figure 2. Main components of device for measuring thermal conductivity of insulating solid materials (Xamán et al. 2009)

The HGP is a type of steady-state method for measuring the thermal conductivity of concrete (Zhang et al. 2015). The exterior of the HGP can be seen in figure 1. The test method requires the test samples to be fixed between hot and cold plates so a constant heat stream can

flow over the test samples. Then the thermal conductivity can be determined by the heat flow and the difference in the mean temperature between the specimen surfaces (Asadi et al. 2018). Figure 2 shows how the specimen is placed between the hot plate and the cold plate. HGP has the same basic principle in measuring the thermal conductivity of the samples. However, it needs additional efforts to cut the sample thin and firmly place the thermal probe with an epoxy (Kim et al. 2003). However, HGP comes with its disadvantages when measuring the thermal conductivity of concrete samples. The HGP method has a significant source of error from the contact resistance between the surface sample and its thermocouple (Al-Ajlan 2006). The HGP method's other disadvantage is the significant amount of time a large temperature gradient needs to be maintained when experimenting.

Two Linear Parallel Probe (TLPP)

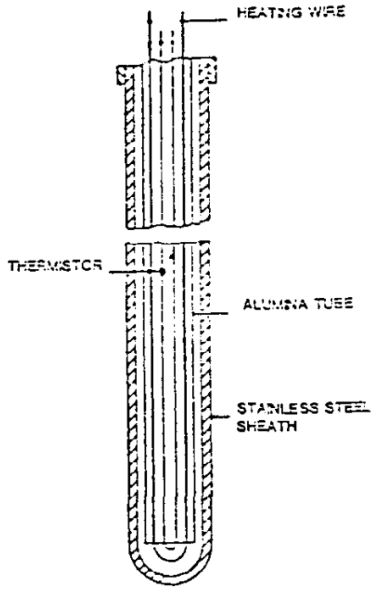

Figure 3. Details of a thermal probe (Morabito 1989)

The TLPP method has been accepted widely in determining the thermal conductivity of concrete though it is the most outdated one compared to the other method. The method can be done by inserting two probes into two parallel holes drilled within the sample concrete. Figure 1 shows the details and components of the thermal probe in TLPP. The probe is made up of stainless steel sheath, and inside of it, there is resistive wire as a heating element for the whole length, while the NTC thermistor that acts as the temperature sensor is placed in the middle of the length (Morabito 1989). During the test, one probe will be the heat source, and the other probe will be the temperature sensor (Kim et al. 2003). The disadvantage of the TLPP method is that it needs lengthy measurements of up to 400 seconds to evaluate the sample's possible thermal drift. In addition, it requires silicon grease to be applied at the probe’s interface (Morabito 1989).

Transient Plane Source (TPS)

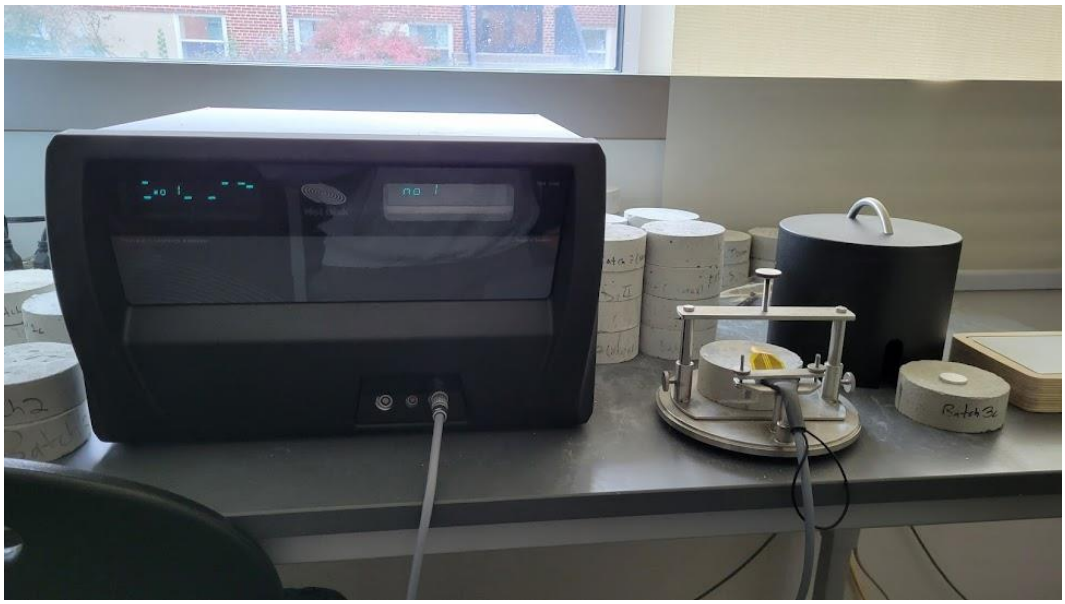

Figure 4. Transient Plane Source device: Hot Disk 1500 at Penn State Harrisburg

Figure 5. TPS Kapton sensor exposed

Figure 6. TPS Kapton sensor sandwiched between the sample

Transient Plane Source (TPS) is a thermal conductivity measurement where a flat sensor is sandwiched between the sample. The temperature is increased with the electrical current that passes through the sensor (Asadi et al. 2018). TPS uses similar principles as TLPP to measure the thermal conductivity of concrete (Kim et al. 2003). This method is a type of transient method and has been used by researchers in determining the changes in the thermal conductivity of sand concretes with the addition of wood shavings (Asadi et al. 2018).

The TPS used for this study is the Hot Disk 1500, manufactured by Hot Disk AB. The exterior of the device can be seen in figure 4. The device consists of the Hot Disk machine itself, the measurement probe, and a connection to the computer to run the experiment using the Hot Disk program. The Hot Disk system is designed to measure thermal transport properties such as thermal conductivity, thermal diffusivity, and the specific heat of a sample (Al-Ajlan 2006). The device utilizes a sensor element shaped like a double spiral, as shown in figure 5. The Kapton sensor functions as both the heat source for increasing the sample's temperature and as the

“resistance thermometer” for measuring the time-dependent temperature increase (Al-Ajlan 2006). Figure 6 shows how the sensor is sandwiched between the two halves of the sample.

Compared to HGP and TLPP, the TPS method has advantages in measuring concrete samples' thermal conductivity. Because the TPS method utilizes a sensor sandwiched between two-cylinder samples. It avoided the significant source of error that HGP encountered from its contact resistance between the thermocouple and sample surface. Furthermore, the measurement time for TPS is significantly faster than both HGP and TLPP as it can determine thermal conductivity in seconds. Besides its measuring time, TPS Hot Disk’s main advantages are its accuracy and wide conductivity measurement range (Al-Ajlan 2006). Though a limitation, it requires the sample to be in a plane surface, as shown in figure 5. TPS method is chosen for this project because its advantages outweigh its limitations compared to the other two methods.

Concrete Mix Design with Foamed Glass Aggregates (FGA)

Figure 7. Dry components of improved insulation concrete, clockwise from top right: Aero Aggregate, OPC, Sandstone, Limestone Aggregate

Concrete plants generally use naturally sourced raw materials to mix into their concrete mixture. This includes the mining and quarrying of limestone, sandstone, and cementitious materials. But as the need for lighter-mass and improved insulation concrete increases, alternative admixtures or aggregate replacement are being sought. One of which is the inclusion of foamed glass aggregate as a partial replacement for limestone coarse aggregate.

Advantages of Foamed Glass Aggregates (FGA)

FGA is considered a lightweight aggregate (LWA), and the concrete with LWA is considered a lightweight concrete. The typical limestone coarse aggregate has a bulk density that ranges from 2376 kg/m^3 to 2478 kg/m^3 (Zhao et al. 2012). The partial replacement of coarse

aggregate with FGA decreases the overall bulk density of the concrete because the bulk density of FGA is significantly lower in the range of 120 to 400 kg/m^3 (Adhikary et al. 2021). In terms of insulating capabilities, limestone coarse aggregates commonly used in concrete have a thermal conductivity of 0.9 – 2.5 W/mK (Çanakci et al. 2007). The FGA has shown a significantly lower thermal conductivity that varies from 0.052 – 0.077 W/mK with a particle size of 0.25 – 16 mm (Adhikary et al. 2021). The lower thermal conductivity is essential in increasing the insulating capability of the concrete wall.

Disadvantages of Foamed Glass Aggregates (FGA)

Figure 8. The exposed porous structure of the FGA is embedded in a concrete sample.

The unique structure of FGA has its disadvantages when included as a component of the concrete mixture. Due to its porous structure and lower mechanical strength, it was reported that the incorporation of FGA decreases the compressive strength of concrete (Adhikary et al. 2021). This porous structure of FGA on a crosscut sample in figure 8. The lightweight concrete using a

portion of FGA with the density of 1000 kg/m^3 can achieve up to 22 MPa of compressive strength and up to 3 MPa of flexural strength (Adhikary et al. 2021). Though the overall strength is lower, all of the concrete mixes that use up to 60% of FGA have achieved the required 28-day design strength and showed a higher early compressive strength due to its alkalis activation (Limbachiya et al. 2012).

FGA is derived from recycled glass with a high amorphous reactive silica content. However, the use of recycled glass in concrete production as a coarse aggregate substitute has been limited due to the destructive nature of combining alkali in cement with amorphous reactive silica in FGA can promote an Alkali-Silica Reaction (ASR) (Adhikary et al. 2021). This combination of alkali and silica reaction has decreased compressive strength and created excessive expansion on concrete (Limbachiya et al. 2012). However, it was also proven that the ASR expansion is still within the threshold value recommended by ASTM C1260 and ASTM C227 (Adhikary et al. 2021). Therefore, this project also includes an ASR test to ensure any expansion of concrete when FGA is included in the mixture.

Chapter 3

Experimental

The research method conducted for this study is through a literature review and laboratory experiments. First, the literature review is being done to improve the understanding of different thermal conductivity testing methods and identify possible modifications for the concrete mixture. Then, a series of concrete sample batches will be cast in the laboratory and given compressive tests. Each batch of samples will have its thermal conductivity measured. The materials in these tests will also be given an Alkali-Silica Reaction (ASR) test to understand their durability.

Concrete Sample Mix Design

Materials

The ingredients obtained for the thermal conductivity test were type I/II Portland cement, blast furnace slag, limestone as the Coarse Aggregate (CA), and natural sand as the Fine Aggregate (FA). The lightweight aggregate (LWA) used for this project is an FGA from Aero

Aggregates of North America, LLC. Aero Aggregates are made from crushed powdered glass from 100% post-consumer recycled glass, then added with a foaming agent and heat.

Table 1. Aggregate Physical Properties

Aggregate types	Bulk Density (kg/m^3)	Specific Gravity	Absorption Capacity (%)
Limestone Gravel	1575	2.81	0.36
Aero Aggregates	248	0.45	32.40
Sandstone	1650	2.56	1.03

Table 1 provides the physical properties of the aggregates. It can be seen that FGA has a lower bulk density compared to limestone and sandstone aggregate. However, its porous structure is well represented by its significantly higher absorption capacity. The mix design also includes admixtures such as Adva Cast 600 as a plasticizer and Daraset 400 as the accelerator. Each mix has a water-to-cement (W/C) ratio = 0.45.

Mixtures

The sample concrete mix design used for the thermal conductivity testing is shown in Table 2. Each batch is a mix design enough for 0.75 ft^3 of concrete. The mix design will be kept constant besides its varied LWA content, which replaces CA in 25%, 50%, 75%, and 100%. A control batch is also included in this study, where it has a 0% replacement of CA for LWA. For batch 2 and batch 3 an additional 10 ml of Adva Cast 600 superplasticizer were added from the constant 38.42 ml to help improve the workability of the mixture. Batch 4 also needed an

additional 15 ml of the superplasticizer to ensure its workability. Figure 9 shows the wet concrete being molded to the cylinder cast. Figure 10 shows the demolded and labeled concrete cylinders after 1-day of curing.

Figure 9. Batch Mixes being cast into cylinder molds

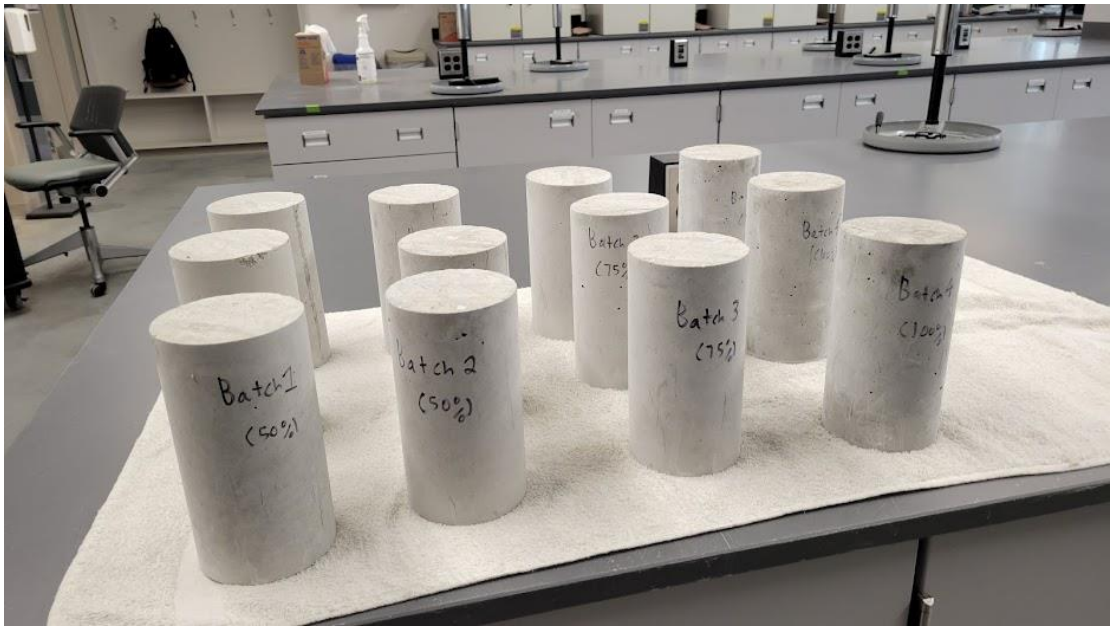

Figure 10. Concrete cylinder samples demolded and labeled

Table 2. Mix Design Details for Concrete Samples.

Materials	Replacement of CA with LWA	Cement (lbs)	Slag (lbs)	LWA (lbs)	CA (lbs)	FA (lbs)	Water (lbs)	Adva Cast 600 (ml)	Daraset 400 (ml)
Control	0%	9.84	9.78	0	43.6	37.53	8.83	38.42	88.25
Batch 1	25%	9.84	9.78	1.60	32.70	37.53	8.83	38.42	88.25
Batch 2	50%	9.84	9.78	3.21	21.80	37.53	8.83	48.42	88.25
Batch 3	75%	9.84	9.78	4.81	10.9	37.53	8.83	48.42	88.25
Batch 4	100%	9.84	9.78	6.41	0	37.53	8.83	53.42	88.25

The ASR mortar bar mix design is described in table 3 based on the design procedure from ASTM C1567. The main difference between the batches in the mix design is their cementitious material content and types of aggregate used. For batches 1A and 2A, it utilized 100% Aero Aggregates instead of the typical limestone CA. However, batch 2A has a partial replacement of its cement with slag to observe the effect of ASR testing on the samples used in the thermal conductivity testing, which were using slag as a cement replacement. Then for batches, 3A, 4A, and 5A and 50/50 content of both limestone CA and Aero Aggregates were used in their mixture. The critical difference between the 3 batches was that 4A and 5A have a partial replacement of cement with slag and 5A has an additional recycled ingredient, Vitro pozzolan.

Table 3. ASR Mix Design

Materials	Batch 1A	Batch 2A	Batch 3A	Batch 4A	Batch 5A
Cement (g)	600	300.8	600	300.8	255.7
Slag (g)		299.2	-	299.2	299.2
Limestone Gravel (g)	-	-	482.9	482.9	482.9
Aero Aggregates (g)	130.4	130.4	65.2	65.2	65.2
Sandstone (g)	581.9	581.9	581.9	581.9	581.9
Water (g)	282	282	282	282	282
Vitro Pozzolan	-	-	-	-	45.1

Based on the grading requirement of aggregates given in the ASTM C1567 for the ASR testing, table 4 gives the amount of mass needed for each particle size of each aggregate type used on each batch. The standard procedures require that the aggregate particle's mass used for the ASR testing should be 10% from the ones that passed sieve #4 and retained on #8, 25% from the ones that passed sieve #8 and retained on #16, 25% from the ones that passed sieve #16 and retained on #30, 25% from the ones that passed sieve #30 and retained on #50, and finally 15% from the ones that passed sieve #50 and retained on #100.

Table 4. ASR Aggregate Grading Requirement

Materials	Batch	Total Mass	Retained on Sieve				
			#8	#16	#30	#50	#100
Limestone Gravel (g)	3A,4A,5A	482.9	48.3	120.7	120.7	120.7	72.4
Aero Aggregates (g)	3A,4A,5A	65.2	6.5	16.3	16.3	16.3	9.8
Aero Aggregates (g)	1A, 2A	130.4	13	32.6	32.6	32.6	19.6
Sandstone (g)	All Batches	581.9	58.2	145.5	145.5	145.5	87.3

Figure 11 shows separating the particle sizes for both the Aero Aggregate and the sandstone using the standard sieving machine. For bigger particles such as Aero Aggregates or Limestone gravel, the jaw crusher machine was used to break the stones into smaller pieces before being sieved and organized according to their size. Figure 12 shows the different sized dry materials being gathered in a bowl before mixing it with water and liquid admixtures.

Figure 11. ASR Aggregate Grading Requirement

Figure 12. ASR test sample’s dry ingredients

Testing Methodology

The concrete samples will be subjected to a compressive strength test. A durability test will also be conducted through the Alkali-Silica Reaction Test (ASR) to observe any relationship between the durability of concrete with the inclusion of recycled-glass LWA in concrete. In addition, ASR will show if any expansion is excessive enough for the concrete to be determined unsafe. Finally, a thermal conductivity test will be conducted using the TPS Hot Disk 1500 on disk concrete samples. Finally, the data results can help determine the relationship of each input parameter, such as measuring time or probing depth, towards the thermal conductivity of each concrete sample. These correlations of different input parameters will be studied to determine practical values for thermal conductivity testing of the concrete mixes.

Compressive Strength Test

Figure 13. Humboldt Hydraulic Press Machine

The compressive test for the concrete samples mentioned on table 3 is done by the 1-day and 28-day compression test based on the standard procedure in ASTM C39. This test was completed using bearing caps and a hydraulic press. Each batch of samples will have 6 concrete cylinders with the diameter of 4 in and height of 8 in. Hence each batch will have 3 cylinders for 1-day testing and another 3 for the 28-day testing. Figure 13 shows the Humboldt hydraulic press machine that is being used to perform the compressive strength test.

Thermal Conductivity Test

All the disk concrete samples are subjected to 28-days curing process before being tested for thermal conductivity. The disk concrete samples being tested are based on the batch mixes

described on table 2. A series of tests will be conducted to determine the effect of different probe depths and measuring time on thermal conductivity values. Thermal conductivity of concrete samples was measured using the Hot Disk TPS 1500 from Thermtest. On each measurement a 6.40 mm radius Kapton sensor is sandwiched between two 38.1 mm (1.5 in) thick x 101.6 mm (4 in) diameter concrete disks. The samples were tested with the room temperature of 20° C.

In order to test the thermal conductivity of the concrete sample, the probing depth and the measuring time need to be included in the probing depth equation where it has two unknowns in a single equation. Not knowing thermal diffusivity is the main issue of this study because it is impractical when calculating the thermal conductivity of a concrete mix as it also relies on the value of the specific heat ahead of time. Hence, the equations need to have an assumption of either one of the probing depth or measurement time values to calculate thermal diffusivity. For this experiment, the results were divided into two categories. First category is the measurement using a varied measuring time for each batch. The second category is the measurement using different locations of the sensor on top of heterogenous concrete surface. Concrete samples using different admixture and aggregate content will be measured and compared to the initial thermal conductivity prediction using the formula from the ACI 122R procedure.

Equation 1. Probing Depth Calculation

$$d_p = 2\sqrt{a * t}$$

$d_p =$ Probing Depth, $a =$ Thermal Diffusivity, $t =$ measurement time

Equation 2. Thermal Diffusivity Calculation

$$a = \frac{k}{\rho C_p}$$

$$k = \text{Thermal Conductivity}, \rho = \text{Density}, C_p = \text{Specific Heat}$$

When using the TPS procedure, it is assumed that the thickness of the sample is infinite for the purpose of heat transfer in between the two-disk sample. This assumption requires that the testing meets its required minimum probing depth. Equation 1 describes that probing depth is dependent on the measurement time, a variable that can be directly input in the Hot Disk program. The measurement time is defined as the amount of time heat is applied towards the disk samples, equivalently the amount of time the sensors will be picking up the data afterwards. Equation 2 describes the thermal conductivity calculation. It is difficult to determine with the initial value for it because it is based on a thermal conductivity value that is unknown before the experiment.

Equation 3. Thermal-Conductivity prediction based of oven-dry density

$$k = 0.5e^{0.02d}$$

$$k = \text{Thermal Conductivity (Btu/h} * \text{ft2)}, \text{and } d = \text{oven} - \text{dry density (lbs/ft3)}$$

In order to calculate using equation 2, an initial value for the thermal conductivity needs to be assumed for each batch mix in table 2 based on the equation 3 that can be found in ACI 122R. Equation 3 can underpredict the thermal conductivity for concrete that contains various types of coarse aggregates. The general value for specific heat of concrete is assumed in equation 2. When using the TPS method, probing depths were calculated using equation 1 for various

measurement times. Commonly, the measured thermal conductivity from the TPS method increase with the longer measurement time. Once the TPS test is run using the initial probing depth and measurement time, the TPS machine will provide a new calculated probing depth as a result of the measured heat transfer data. The probing depth calculated from equation 1 will not match the final probing depth calculated from the Hot Disk 1500 because of the assumption used to calculate thermal diffusivity is attributed to the homogenous composition of the concrete mix.

Figure 14. TPS Sensor embedded in a powder of aggregate

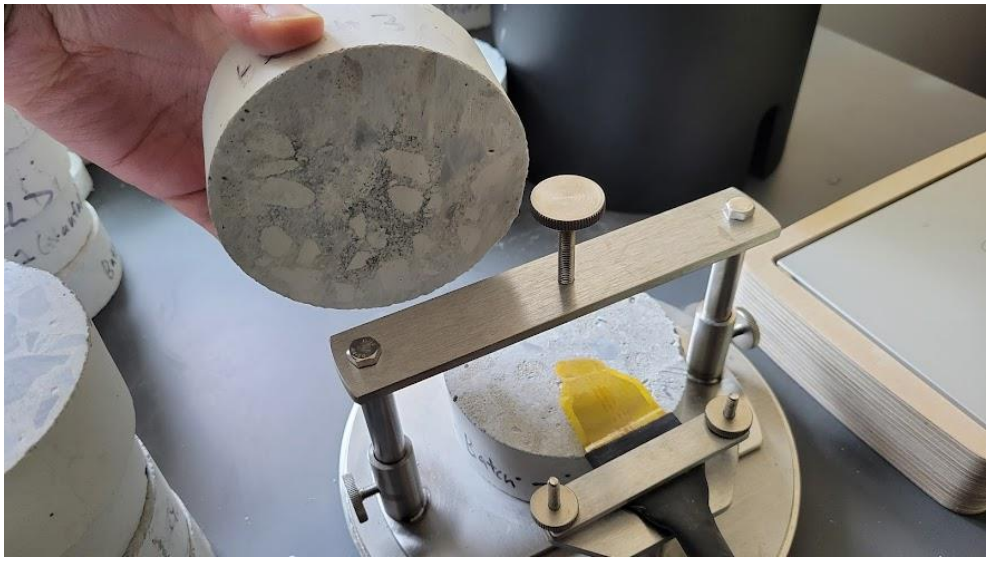

Figure 15. Kapton sensor on exposed Aero Aggregate surface

This project conducted multiple iterations for each batch mix until the input probing depth matched the Hot Disk 1500 probing depth. Once it is matched, the thermal conductivity of the sample is recorded. Measurement time of 40 s has provided similar and reliable results compared to other measurement times that were input. The TPS method were used in this project to determine the thermal conductivity of both the individual concrete components and concrete samples. The individual concrete components mentioned are such as coarse aggregates, fine aggregates, and cementitious material. These components' thermal conductivity will be measured by embedding the TPS sensor into a container of aggregate powder obtained through a sieving process as can be seen on figure 14. For coarse aggregates such as gravel and Aero Aggregate, thermal conductivity was also recorded through placing the Kapton sensor on the exposed surface of these aggregates in the concrete samples themselves. This sensor placement can be seen on figure 15 and the result of thermal conductivity recording is utilized to help compute the prediction equation.

Equation 4. Prediction Equation

$$\boldsymbol{k = k_p \sum_{i=1}^{n} \left[\frac{v_i^{\frac{2}{3}}}{v_i^{\frac{2}{3}} - v_i + \left(\frac{v_i}{\left(\frac{k_i v_i^{\frac{2}{3}}}{k_p} \right) + 1 - v_i^{\frac{2}{3}}} \right)} \right]}$$

k_p = paste thermal conductivity, k_i = thermal conductivity of aggregate i, v_i = volume

Equation 4, also provided in ACI 122R, is a two-phase model equation for predicting thermal conductivity of concrete (Valore 1980). The equation is computed based on the unit cubic of concrete where the aggregate is being surrounded from all side by paste with a constant thickness of $0.5\left(1 - {v_i}^{1/3}\right)$. From using the cubic model, equation 4 can account for thermal bridges in between the different thermal conductivities of the paste and aggregate. As given on ACI 122R, the thermal conductivity calculated using equation 4 are close in comparison to using equation 3 for concrete densities with ≤ 1922.22 kg/m^3 (120 lb/ft^3).

Equation 5. Unifying Model Equation (UME)

$$k = \sum_{i=1}^{m} v_i k_i \frac{d_i k^*}{(d_i - 1)k^* + k_i} * \left(\sum_{i=1}^{m} v_i \frac{d_i k^*}{(d_i - 1)k^* + k_i} \right)^{-1}$$

Equation 6. Calculating k*

$$k^* = \frac{v_3 k_3 \frac{d_3 k_4}{(d_3 - 1)k_4 + k_3} + v_4 k_4 \frac{d_4 k_4}{(d_4 - 1)k_4 + k_4}}{v_3 \frac{d_3 k_4}{(d_3 - 1)k_4 + k_3} + v_4 \frac{d_4 k_4}{(d_4 - 1)k_4 + k_4}}$$

This project also utilizes the prediction equation using Unifying Model Equation (UME) given by equation 5 to predict the thermal conductivity of the concrete sample (Wang et al. 2006). Given in equation 5, the v_i = volume fraction of concrete component (i.e., gravel ($i = 1$), FGA ($i = 2$) cement matrix ($i = 3$), air voids ($i = 4$)), k_i = thermal conductivity of concrete component *i*, d_i = shape factor of concrete component *i*, m = number of concrete components, and k^* is given in equation 6. The physical interpretation of the d_i is debated, though numerous works has considered it as a combination of component's shape and number of Euclidean dimensions. The common approach, as recommended by previous studies, is to take $d_i = 3$, which represents a spherical dispersed phase (Wang et al. 2006).

Due to the ambiguity in the physical interpretation of the variable, this project will assume $d_i = 3$. The variable k^* in equation 6 represents the combined thermal conductivity of the cement matric and air. The variable also is part of the two-phase system assumption for the model between the cement matrix/air and the coarse aggregates. It is assumed for this project that any effects coming from air voids were not considered in the prediction equation. The computed air content value from the concrete mixes based on the theoretical density against its measured weight as outlined in ASTM C138 was not significant enough to make any important difference in the prediction equation calculations. The experimental air content test was not conducted for this project because the accuracy of the test used for lightweight concrete outlined in ASTM

C173 is highly subjective. It is noted that the result of this tests is subjective because of the level of difficulty in performing the volumetric procedures as required by the given standards.

Alkali-Silica Reaction (ASR) Test

Figure 16. Los Angeles abrasion crusher machine

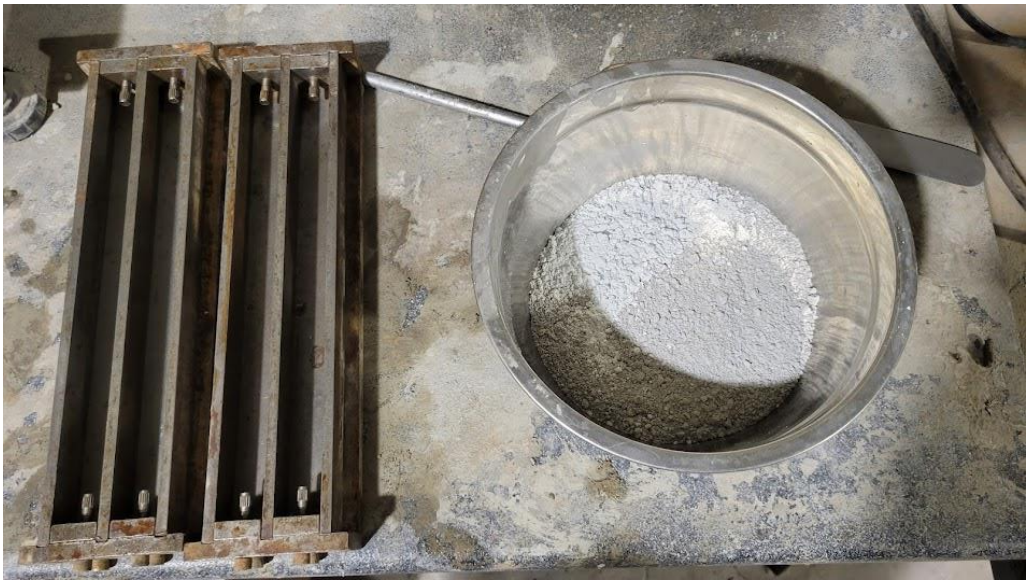

Figure 17. ASR test metal mortar molds with the dry ingredients for the sample

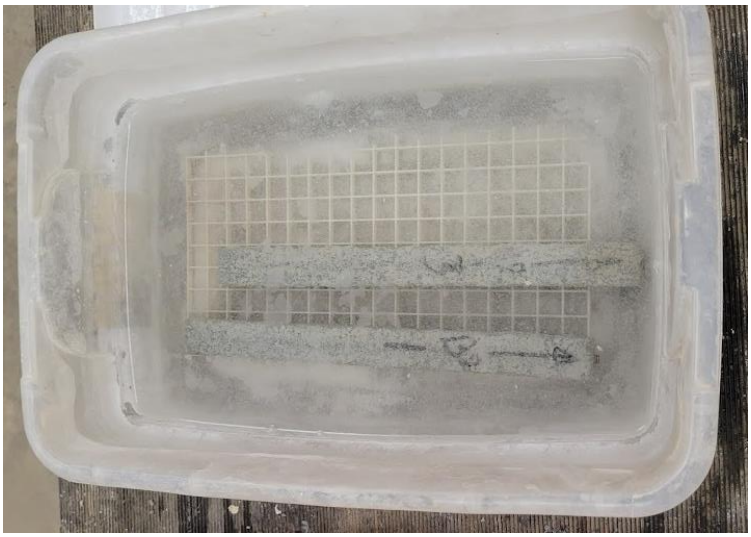

Figure 18. Mortar bars submerged in NaOH bath for the ASR test

The ASR test performed on this project is based on the accelerated mortar bar test outlined in ASTM C1567. The mix design for the ASR test is outlined in table 3 and the grading requirements from ASTM C1567 is reflected in table 4. To obtain the correct grading

requirement from larger size gravels, the aggregates were crushed using the Los Angeles Abrasion machine as can be seen on figure 16. Inside the rotating steel drum, multiple steel balls crush the gravel into smaller particle size.

For each batch, three 25 x 25 x 250 mm mortars were prepared with embedded gage studs at the ends to facilitate length measurement (Shafaatian et al. 2013). The metal mold for the mortar is shown on figure 17. For this accelerated method, after 24 hours of water curing, the mortar bars were demolded and stored submerged inside a container with 1N NaOH at 80^{o}C for 14 days (Li et al. 2019). Figure 118 shows the example of how the concrete mortar samples are submerged inside a NaOH bath. The mortar bars are then measured for signs of expansion with a digital comparator with an accuracy of 0.0025 mm.

Chapter 4

Result and Discussion

Preliminary Tests

Concrete Strength Properties

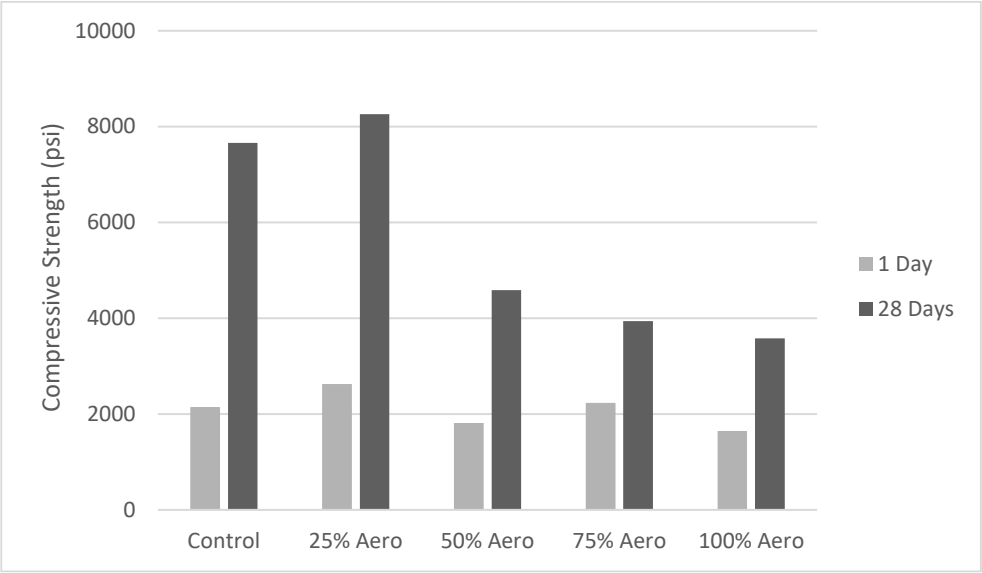

Figure 19. Concrete Cylinder Compressive Strength Result

The 1-day and 28-day compression strength results from the mixes in table 2 are shown in figure 19. The 1-day compression test shows that there is not a significant difference between batches that has an increased amount of FGA content, though there is no consistent trend. Out all of the batches, only mixes with 50% FGA and 100% FGA that are slightly below the 2,000-psi requirement. The 28-day test shows a more consistent trend where there is a decrease in the compressive strength with the increase of FGA content above 25%. The 28-day compression strength results are directly correlated with the amount of FGA Aero Aggregates used in the mix

once a significant amount of hydration is achieved. The 25% FGA concrete mix shows an improved compressive strength where it achieved peak average strength of 8,262.40 psi compared to the control batch of 7,662.34 psi. In comparison, the batch with 100% FGA shows a significantly lowered compressive strength where it only peaked at an average of 3,583.13 psi, which is less than half of the control batch's strength. Table 5 shows the full results from the 1-day compressive strength, and table 6 shows the 28-day compressive strength of the concrete sample cylinder. Figure 18 shows an example of how the concrete cylinder sample is cracked when given a compression force. Figure 21 shows the crosscut interior of the concrete cylinder's sample. On the figure, the coarse aggregate is identified as dark-colored gravel and the light-colored coarse aggregates are Aero Aggregates FGA. One unique observation during this project is when the crosscut of each samples shows the distribution of its coarse aggregate. Figure 21 shows that the majority of FGA are concentrated on the top side of the cylinder and the heavier limestone gravels are at the bottom half. This is possibly attributed to the density of the material when during the concrete mixing, the lighter FGA floats above the gravel.

Table 5. 1-Day Compressive Strength Test

Name	FGA (%)	Sample 1	Sample 2	Sample 3	Average
		Strength (psi)	Strength (psi)	Strength (psi)	Strength (psi)
Control	0%	2145.11			
Batch 1 (25%)	25%	2373.88	2828.50	2676.27	2626.22
Batch 2 (50%)	50%	2074.03	1636.59	1730.17	1813.60
Batch 3 (75%)	75%	2218.14	2015.62	2462.92	2232.23
Batch 4 (100%)	100%	1628.16	1440.67	1872.14	1646.99

Table 6. 28-Day Compressive Strength Test

Name	FGA (%)	Sample 1	Sample 2	Sample 3	Average
		Strength (psi)	Strength (psi)	Strength (psi)	Strength (psi)
Control	0%	7662.34			
25% Aero	25%	8221.39	8557.76	8008.04	8262.40
50% Aero	50%	4221.03	4661.73	4869.58	4584.11
75% Aero	75%	4076.75	3459.15	4284.29	3940.07
100% Aero	100%	3885.85	3339.55	3524.01	3583.13

Figure 20. Compressive Strength Testing on Concrete Cylinder Samples

Figure 21. Crosscut of the concrete cylinder sample

ASR Test Result

Figure 22. ASR test concrete samples

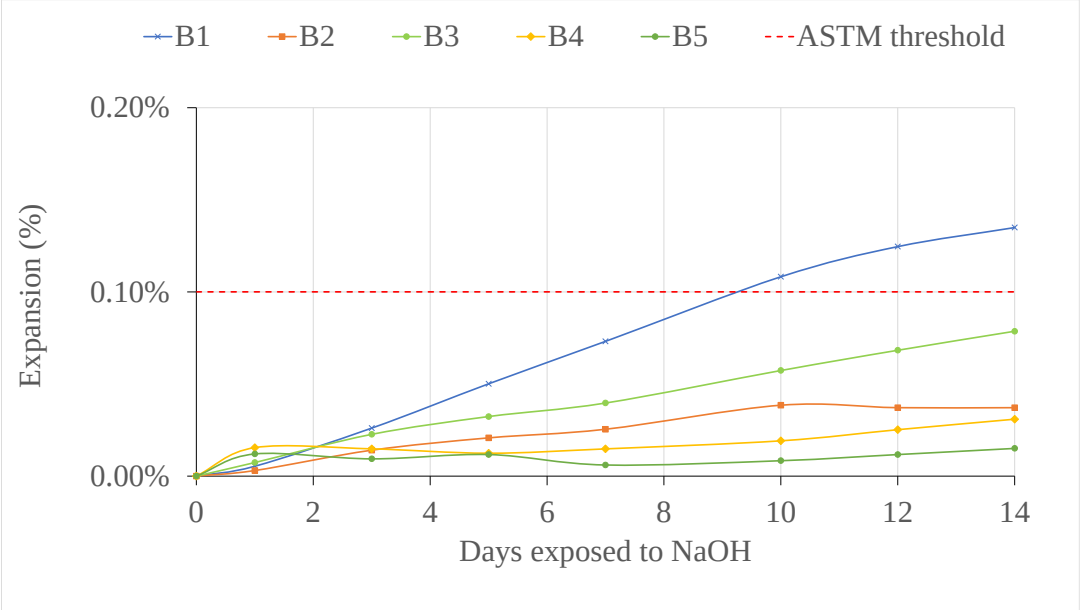

Figure 23. ASR Test Result in Comparison with ASTM Standard

For 14 days the mortars shown in figure 22 are submerged in a NaOH. The mortars' mixture is based on the description given on table 3. Measurements of its expansion is done on day 0, 1, 3, 5, 7, 10, 12, and 14. The data points of the expansion measurement are shown on table 7 and interpreted on figure 23. Figure 23 also shows the ASTM threshold of 0.10% in expansion. Based on the batch mixtures, four out five mixes managed to stay below the maximum threshold (batch 2, 3, 4, and 5). Those batches are mortar mixes has 50% Aero Aggregate FGA replacement and/or 50% cement replacement using slag. Batch 2 mix that uses 100% Aero Aggregate FGA replacement managed to stay below the 0.10% threshold with the addition of 50% cement replacement with slag. The only mix that goes beyond the threshold is batch 1 that achieved 0.13% of expansion after 14 days. It should be noted that batch 1 uses 100% Aero Aggregate replacement for coarse aggregate and did not use any slag as an admixture to its cement.

Table 7. Rate of ASR Expansion (%)

	Day 0	**Day 1**	**Day 3**	**Day 5**	**Day 7**	**Day 10**	**Day 12**	**Day 14**
B1	0.00%	0.01%	0.03%	0.05%	0.07%	0.11%	0.12%	0.13%
B2	0.00%	0.00%	0.01%	0.02%	0.03%	0.04%	0.04%	0.04%
B3	0.00%	0.01%	0.02%	0.03%	0.04%	0.06%	0.07%	0.08%
B4	0.00%	0.02%	0.01%	0.01%	0.01%	0.02%	0.03%	0.03%
B5	0.00%	0.01%	0.01%	0.01%	0.01%	0.01%	0.01%	0.02%

Thermal Conductivity Test

Thermal Conductivity of Individual Concrete Components

Table 8. Thermal conductivity (W/mK) of concrete mix materials

Materials	**Emerged**	**Surface Exposure**
Cement	0.53	
Slag	0.35	Cement Matrix = 1.94
Sandstone	0.34	
Aero Aggregates	0.12	0.79
Limestone Gravel	0.39	2.68

Before going through the input parameters of thermal conductivity measurements, this project goes through the thermal conductivity measurement of individual concrete components. Table 8 shows the thermal conductivity for the materials cement, slag, sandstone, Aero Aggregate, and limestone gravel. The measurement was done in two different ways. First is by having the Kapton sensor emerged in containers of sieved aggregate as can be seen on figure 14, and secondly is by placing the sensor on the concrete sample's surface that is exposed with the aggregate as can be seen on figure 5. It is observed from the test that the thermal conductivity of the emerged sensor is less compared to the exposed sensor to aggregate's surface on the concrete sample. Although the sensor is being emerged in the small grains of the aggregate, it is possible that the lower thermal conductivity measurement is because of the air surrounding the sensor instead of having it sandwiched in between two solid materials.

Figure 24. A container of slag powder with an emerged Kapton sensor

It is noticeable in figure 24 where the slag powder is not compacted, which means pockets of air exist around the sensor. Based on table 8, the emerged thermal conductivity for Aero Aggregate FGA (0.12 W/mK) does not fall into the reported range of 1.3 -2.3 W/mK in ACI 122R. The same goes with sandstone (0.34 W/mK) which did not fall into its reported range of 0.052 – 0.077 W/mK (Adhikary et al. 2021). Different could be said for gravel, even though the emerged measurement was lower than the expected range (only 0.39 W/mK), the surface exposure measurement (2.68 W/mK) did fall into the expected range for limestone of 1-3 W/mK as reported in ACI 122R.

Thermal Conductivity by Location and Measuring Time

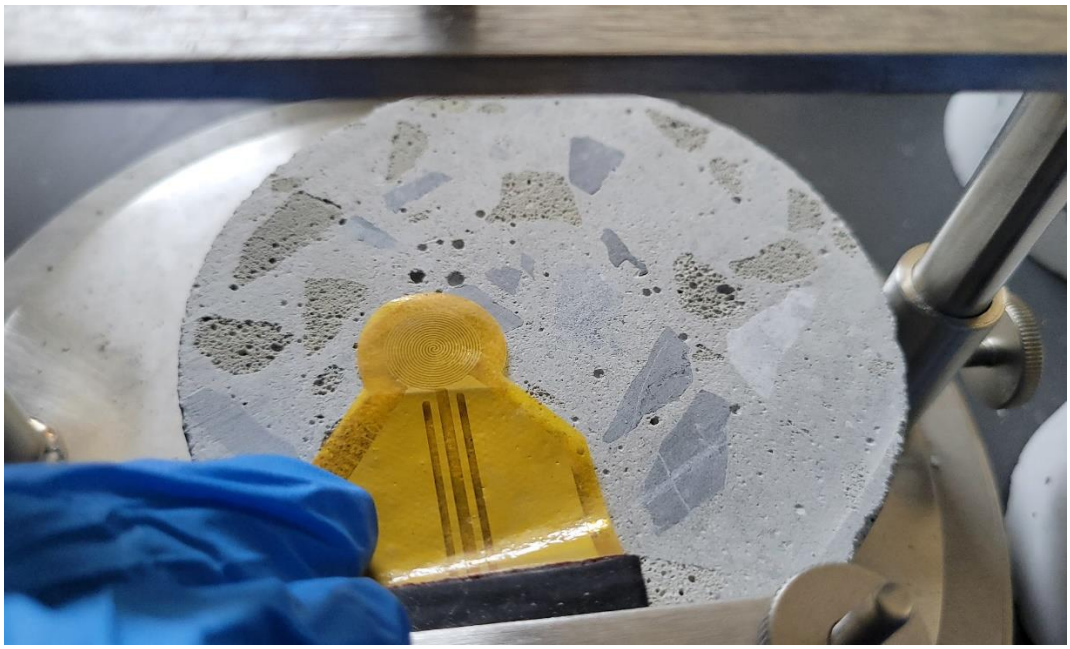

Figure 25. Thermal conductivity testing by location of different aggregates

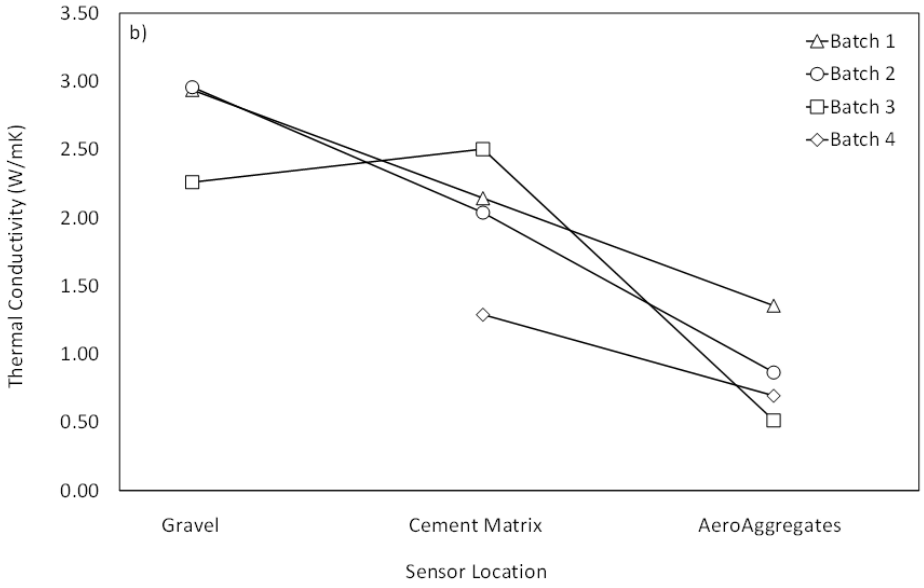

Figure 26. Thermal conductivity using TPS method by variable sensor location

From this project it is understood that the sensor placement is a significant factor in measuring the thermal conductivity of the sample based on the mix design of table 2. It can be

seen on figure 25 that the Kapton sensor is being moved around directly over the gravel, Aero Aggregate, or the cement matrix. Appendix A shows a more detailed information of input parameter and measured thermal conductivity for each batch's samples. When the Kapton sensor is placed on the gravel, the measured thermal conductivity is within the reported range for normal weight concrete. But when the sensor is moved over to the Aero Aggregate, for batch 3 and 4 it will change the thermal conductivity wo within the reported range for lightweight concrete (0.2 – 1.9 W/mK) and within reported ranges for FGA concrete (0.075 – 0.847 W/mK) (Adhikary et al. 2021). In comparison, batch 2 did not fall within the FGA concrete range with the thermal conductivity of 0.87 W/mK. Figure 26 shows the data interpretation of thermal conductivity measurement based on the variable sensor location. It can be seen from the figure that placing the sensor on the Aero Aggregate can lower the thermal conductivity compared to placing the sensor on either the gravel or the cement matrix.

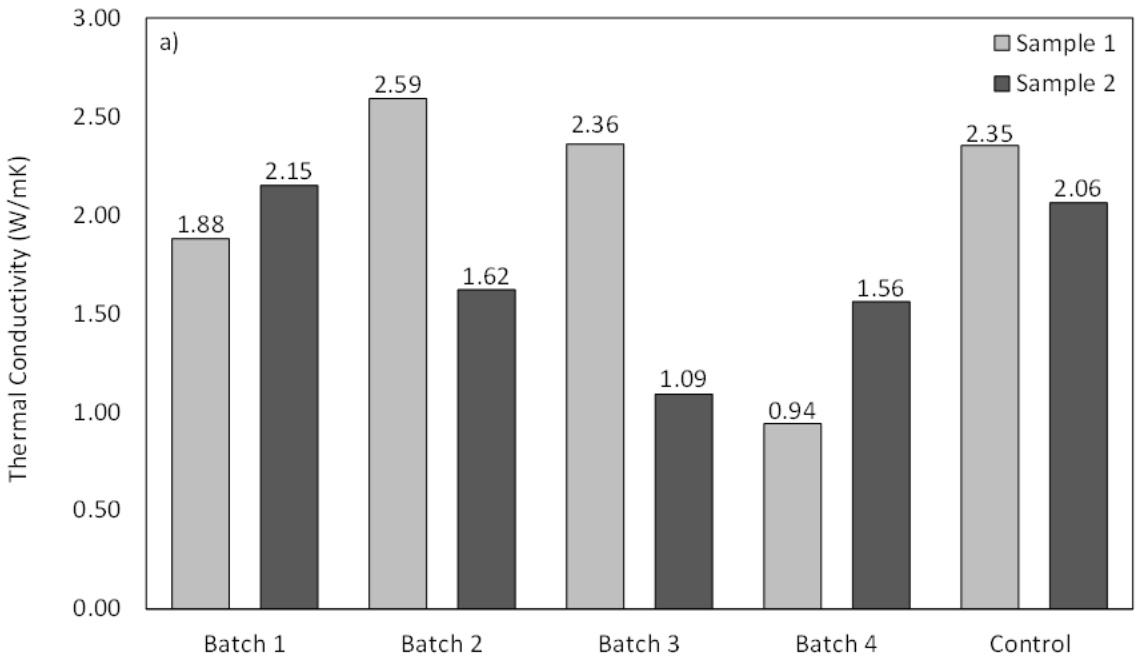

Figure 27. Thermal conductivity using TPS method by placing sensor in sample center

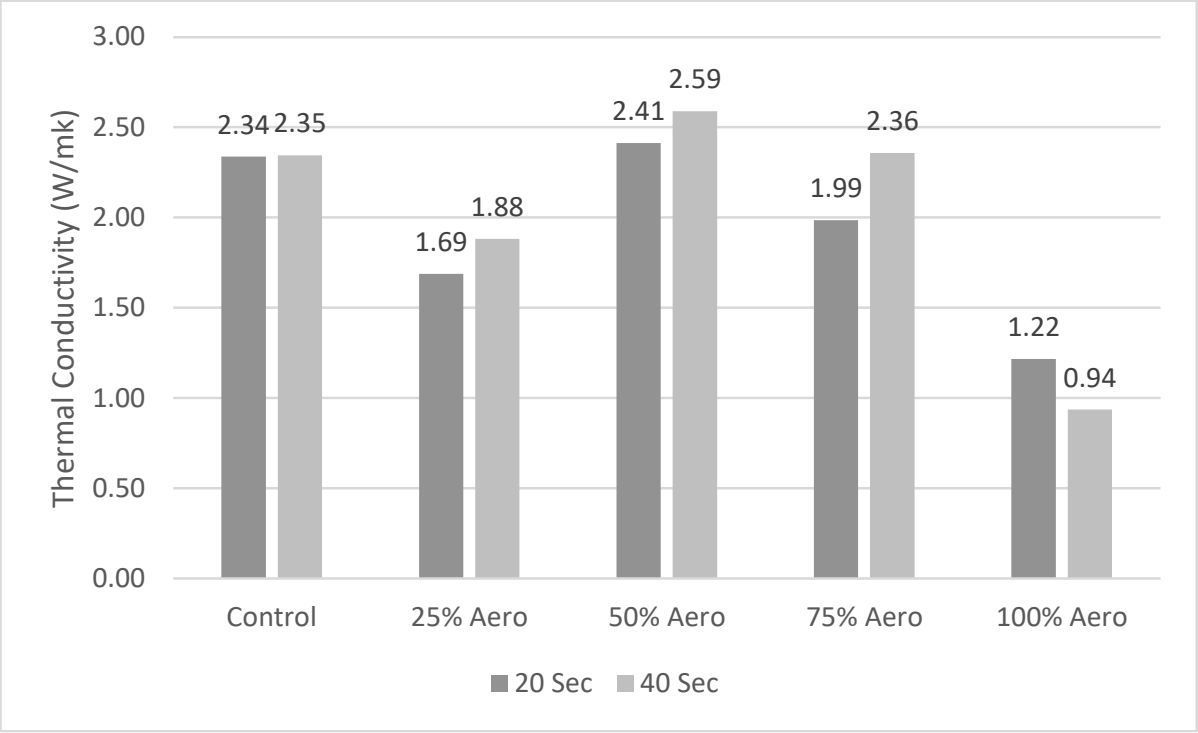

Figure 28. Thermal conductivity test result based on measuring time

It should be noted that when the sensor is placed consistently in the center, there would be a lot of variability for the measurement of thermal conductivity of concrete mix. Figure 27 shows the thermal conductivity average measurement when placed in the center of the sample. There is no consistent trend on figure 27 to show the effect of the inclusion of FGA towards the thermal conductivity. Showing the thermal conductivity data as a bar chart from makes it less informative in comparison with figure 26 where the data is interpreted as a curve of different data points of location measurements. Figure 28 shows the thermal conductivity reading based of the measuring time of 20 sec and 40 sec. The bar chart shows a slight trend where increase of measuring time could be attributed to higher reading of thermal conductivity. Although, batch 4 in this measurement became an outlier as it has a lower thermal reading on 40 sec.

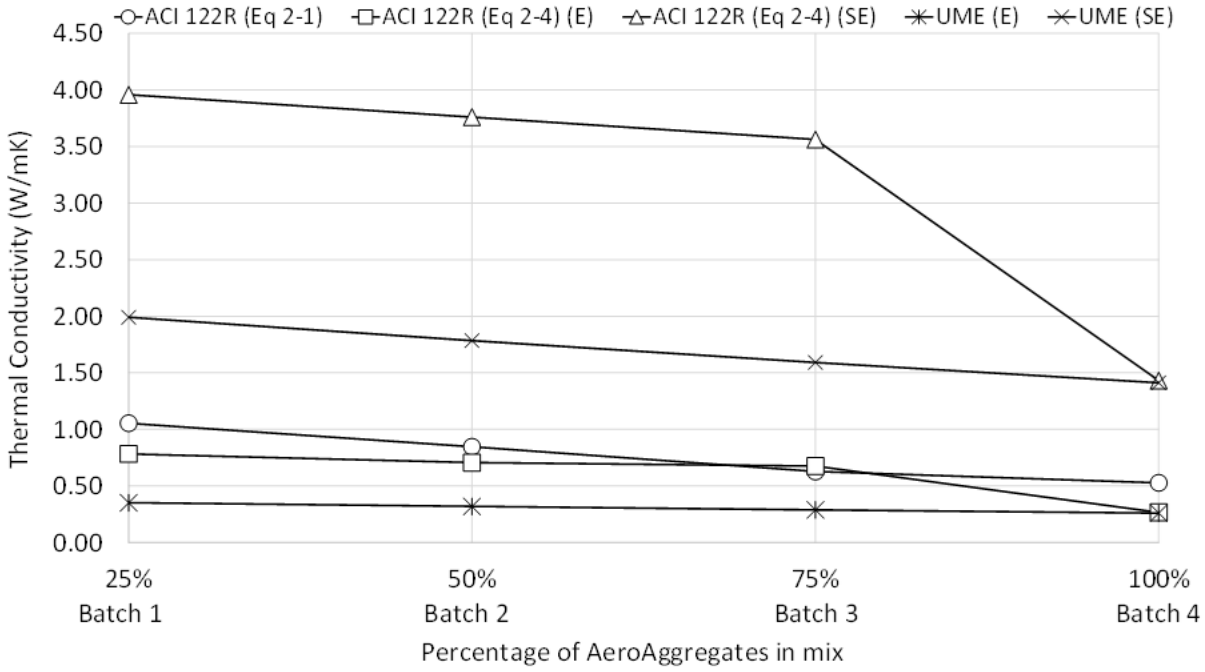

Figure 29. Thermal conductivity using prediction equation

Figure 29 shows the thermal conductivity for each mix from table 2 based on the prediction equations. The thermal conductivity values were predicted using equation 3 from Eq 2-4 of ACI 122R, equation 4 based on the cubic model from (Valore 1980) as outlined in Eq. 2-4 of (ACI/TMS Committee 122 2014), and the UME (Wang et al. 2006) provided in equation 5 and 6. Within the graph on figure 29, the use of surface exposed sensor is denoted by "SE" and the emerged sensor is denoted by "E". Figure 29 shows that all of the curves, with the exception of SE, fall between the range of 0.25 – 1.05 W/mK which is within the general range of lightweight concrete (0.2 – 1.9 W/mK) and some in the reported ranges for FGA concrete (0.075 – 0.847 W/mK).

It can be seen from the graph in figure 29 that there is a noticeable difference between cubic model and UME when predicting thermal conductivity using "SE" sensor vs. the "E"

sensor. This is a direct consequence of having different thermal conductivity values of individual components that were mentioned in table 8. It is noted that using the “E” sensor values in the prediction values have produced more reasonable thermal conductivity results compared to reported values. This would be in contrast from the thermal conductivity of individual concrete components where the “SE” sensor provided more reasonable values, with FGA as an exception. The graph shows that there is a significant change in the cubic model prediction when it transitions between batch 3 and batch 4. This is because batch 3 has 25% gravel and batch 4 has none. The cubic model equation does not show a consistent trend when an individual concrete component is removed from its calculation. In comparison, the other three prediction equation shows a consistent trend on its curve when the FGA content is increased between the batches.

Chapter 5

Conclusion

The study from this project presents the results of an experimental investigation of the input parameters of thermal conductivity measurements of sustainable concrete incorporated with FGA. The findings and observation are summarized below:

- For the TPS method, it is more accurate to measure thermal conductivity of a material by using surface exposed sensor compared to emerged sensor, even though surface exposed sensor has its own limitations when it placed on a highly porous material.

- Sensor placement on the sample has a significant effect on the thermal conductivity measurement of the material. When the sensor was located on a gravel within the concrete disk it shows a higher thermal conductivity and FGA showing a lower value compared to the reported normal weight concrete value.
- Only batch 2 with 25% FGA shows a higher 1-day and 28-day compressive strength compared to the control batch. The rest of the batches (50%, 75%, and 100% FGA) shows a decrease in compressive strength as low as half of the control batch strength.
- The inclusion of FGA will not promote excessive ASR expansion when incorporated with 50% slag cement replacement or/and 50% gravel as coarse aggregate. Only mortar samples with 100% FGA without any slag cement replacement shows expansion beyond the ASTM threshold of 0.10%.
- The increase of time measurement shows a slight increase in thermal conductivity value for every batch except for batch 4 that has 100% FGA coarse aggregate replacement.
- This shows that a single value of thermal conductivity would not be appropriate to represent the thermal behavior of concrete mixtures that has multiple variants of coarse aggregates. A range curve such as of figure 26 would better represent the concrete.
- The prediction equations could not fully represent the thermal behavior of concrete mixes when used to calculate a single thermal conductivity value. Although, the cubic equation from ACI 122R (Eq. 2-4) can be an exception as it shows a consistent linear trend for calculated thermal conductivity between batches.

Appendix A

Thermal Conductivity Measurement by Location

Table 9. Batch 1 (25 Aero/75 Limestone) Sample 1

T (sec)	D (mm)	K (W/mk)	D Input	Location
40	14.9	1.522	15.5	gravel
40	15.4	1.555	15.5	gravel
40	13.7	2.155	15.5	gravel
40	13.8	1.677	13.7	paste
40	23.6	0.9014	13.8	**aero**

Note: Batch 1 is segregated where each half cylinder only contains either gravel or FGA

Table 10. Batch 1 (25 Aero/75 Limestone) Sample 2

T (sec)	D (mm)	K (W/mk)	D Input	Location
40	13.8	2.937	15.5	gravel
40	14.6	2.144	13.8	paste
40	24.1	1.356	14.6	**aero**

Table 11. Batch 2 (50 Aero/50 Limestone) Sample 1

T (sec)	D (mm)	K (W/mk)	D Input	Location
40	12	2.72	15.5	gravel
40	13.2	2.173	12	paste
40	35.3	0.7518	13.2	**aero**

Table 12. Batch 2 (50 Aero/50 Limestone) Sample 2

T (sec)	D (mm)	K (W/mk)	D Input	Location
40	12.9	3.196	18.7	gravel
40	**9.58**	**1.903**	12.9	paste
40	14.2	0.9816	9.58	**aero**

Table 13. Batch 3 (75 Aero/25 Limestone) Sample 1

T (sec)	D (mm)	K (W/mk)	D Input	Location
40	12.6	**2.295**	15.6	gravel
40	13.7	2.319	12.6	paste
40	27.4	0.3428	13.7	aero

Table 14. Batch 3 (75 Aero/25 Limestone) Sample 2

T (sec)	D (mm)	K (W/mk)	D Input	Location
40	**11**	**2.227**	19.3	gravel
40	13.5	2.688	11	paste
40	21.9	0.6871	13.5	aero

Table 15. Batch 4 (100 Aero Aggregates) Sample 1

T (sec)	D (mm)	K (W/mk)	D Input	Location
40	N/A	N/A	N/A	gravel
40	8.88	0.7197	10.1	paste
40	15.6	0.6299	8.88	aero

Table 16. Batch 4 (100 Aero Aggregates) Sample 2

T (sec)	D (mm)	K (W/mk)	D Input	Location
40	N/A	N/A	N/A	gravel
40	11.1	1.861	11.9	paste
40	19	0.761	11.1	aero

BIBLIOGRAPHY

ACI/TMS Committee 122. 2014. *ACI 122R-14: Guide to Thermal Properties of Concrete and Masonry Systems*.

Adhikary, S. K., D. K. Ashish, and Ž. Rudžionis. 2021. "Expanded glass as lightweight aggregate in concrete – A review." *J. Clean. Prod.*, 313: 127848. https://doi.org/10.1016/j.jclepro.2021.127848.

Al-Ajlan, S. A. 2006. "Measurements of thermal properties of insulation materials by using transient plane source technique." *Appl. Therm. Eng.*, 26 (17): 2184–2191. https://doi.org/10.1016/j.applthermaleng.2006.04.006.

Asadi, I., P. Shafigh, Z. F. B. Abu Hassan, and N. B. Mahyuddin. 2018. "Thermal conductivity of concrete – A review." *J. Build. Eng.*, 20: 81–93. https://doi.org/10.1016/j.jobe.2018.07.002.

Çanakci, H., R. Demirboğa, M. Burhan Karakoç, and O. Şirin. 2007. "Thermal conductivity of limestone from Gaziantep (Turkey)." *Build. Environ.*, 42 (4): 1777–1782. https://doi.org/10.1016/j.buildenv.2006.01.011.

del Coz Díaz, J. J., P. J. García Nieto, C. Betegón Biempica, and M. B. Prendes Gero. 2007. "Analysis and optimization of the heat-insulating light concrete hollow brick walls design by the finite element method." *Appl. Therm. Eng.*, 27 (8): 1445–1456. https://doi.org/10.1016/j.applthermaleng.2006.10.010.

Demirboğa, R., and R. Gül. 2003. "The effects of expanded perlite aggregate, silica fume and fly ash on the thermal conductivity of lightweight concrete." *Cem. Concr. Res.*, 33 (5): 723–727. https://doi.org/10.1016/S0008-8846(02)01032-3.

Kim, K.-H., S.-E. Jeon, J.-K. Kim, and S. Yang. 2003. "An experimental study on thermal conductivity of concrete." *Cem. Concr. Res.*, 33 (3): 363–371. https://doi.org/10.1016/S0008-8846(02)00965-1.

Li, Z., R. J. Thomas, and S. Peethamparan. 2019. "Alkali-silica reactivity of alkali-activated concrete subjected to ASTM C 1293 and 1567 alkali-silica reactivity tests." *Cem. Concr. Res.*, 123: 105796. https://doi.org/10.1016/j.cemconres.2019.105796.

Limbachiya, M., M. S. Meddah, and S. Fotiadou. 2012. "Performance of granulated foam glass concrete." *Constr. Build. Mater.*, 28 (1): 759–768. https://doi.org/10.1016/j.conbuildmat.2011.10.052.

Morabito, P. 1989. "Thermal conductivity and diffusivity measurements by the transient two linear and parallel probe method." *Thermochim. Acta*, 148: 513–520. https://doi.org/10.1016/0040-6031(89)85255-4.

Nguyen, T.-D., D.-T. Pham, and M.-N. Vu. 2019. "Thermo-mechanically-induced thermal conductivity change and its effect on the behaviour of concrete." *Constr. Build. Mater.*, 198: 98–105. https://doi.org/10.1016/j.conbuildmat.2018.11.146.

Sargam, Y., K. Wang, and J. E. Alleman. 2020. "Effects of Modern Concrete Materials on Thermal Conductivity." *J. Mater. Civ. Eng.*, 32 (4).

Sengul, O., S. Azizi, F. Karaosmanoglu, and M. A. Tasdemir. 2011. "Effect of expanded perlite on the mechanical properties and thermal conductivity of lightweight concrete." *Energy Build.*, 43 (2): 671–676. https://doi.org/10.1016/j.enbuild.2010.11.008.

Shafaatian, S. M. H., A. Akhavan, H. Maraghechi, and F. Rajabipour. 2013. “How does fly ash mitigate alkali–silica reaction (ASR) in accelerated mortar bar test (ASTM C1567)?” *Cem. Concr. Compos.*, 37: 143–153. https://doi.org/10.1016/j.cemconcomp.2012.11.004.

Uysal, H., R. Demirboğa, R. Şahin, and R. Gül. 2004. “The effects of different cement dosages, slumps, and pumice aggregate ratios on the thermal conductivity and density of concrete.” *Cem. Concr. Res.*, 34 (5): 845–848. https://doi.org/10.1016/j.cemconres.2003.09.018.

Valore, R. C. 1980. “Calculations of U-Values of Hollow Concrete Masonry.” *Concr. Int.*, 2 (2): 40–63.

Wang, J., J. K. Carson, M. F. North, and D. J. Cleland. 2006. “A new approach to modelling the effective thermal conductivity of heterogeneous materials.” *Int. J. Heat Mass Transf.*, 49 (17): 3075–3083. https://doi.org/10.1016/j.ijheatmasstransfer.2006.02.007.

Xamán, J., L. Lira, and J. Arce. 2009. “Analysis of the temperature distribution in a guarded hot plate apparatus for measuring thermal conductivity.” *Appl. Therm. Eng.*, 29 (4): 617–623. https://doi.org/10.1016/j.applthermaleng.2008.03.033.

Yun, T. S., Y. J. Jeong, T.-S. Han, and K.-S. Youm. 2013. “Evaluation of thermal conductivity for thermally insulated concretes.” *Energy Build.*, 61: 125–132. https://doi.org/10.1016/j.enbuild.2013.01.043.

Zhang, W., H. Min, X. Gu, Y. Xi, and Y. Xing. 2015. “Mesoscale model for thermal conductivity of concrete.” *Constr. Build. Mater.*, 98: 8–16. https://doi.org/10.1016/j.conbuildmat.2015.08.106.

Zhao, H., W. Sun, X. Wu, and B. Gao. 2012. “The effect of coarse aggregate gradation on the properties of self-compacting concrete.” *Mater. Des.*, 40: 109–116. https://doi.org/10.1016/j.matdes.2012.03.035.

ACADEMIC VITA

EDUCATION

Bachelor of Science in Civil Engineering (Schreyer Honors College) — **May 2022 (expected)**
The Pennsylvania State University – Capital College, Harrisburg, PA

CGP

A: 3.91/4.00

AWARDS

Student Engagement Network Grant ($2000) – Afghan Refugee Project – Penn State	**2022**
Dean's List – Penn State Harrisburg (every semester)	**2018 – 2022**
Ardeth and Norman Frisbey Int'l Undergraduate Student Leadership Award – Penn State	**2021**
Drawdown Sustainability Research Grant	**2021**
Multi-Campus Research Experience for Undergraduates Grant ($4,200) – Penn State	**2020, 2021**
Honorable Mention: Startup Challenge - Penn State Harrisburg	**2019**
Outstanding Community Service Award – Global Ambassadors Program	**2019**
President's Freshman Award – Penn State Harrisburg	**2019**
Chevron Scholastic Award Scholarship ($50,000 annual scholarship)	**2017**
Bronze Medalist at Southeast Asian Mathematical Olympiad (SEAMO)	**2017**

RESEARCH EXPERIENCE

Undergraduate Student Researcher – *Thermal Conductivity of Lightweight Concrete* — **May 2021 – August 2021**
Drawdown Project, Penn State

- Conducted concrete lab testing for compressive strength, thermal conductivity, and alkali-silica reaction test according to ASTM standards
- Operated civil lab machines such as the sieve shaker, jaw crusher, transient-plane source machine, hydraulic press, and mixing concrete mortars
- Written and analyzed data on sustainable energy-conserving concrete walls

Undergraduate Student Researcher – *Self-Consolidating Concrete (SCC)* — **May 2020 – August 2020**
Virtual Multi-Campus Research Experience for Undergraduates, Penn State

- Conducted literature review on 50+ journal papers with the topic of Self-Consolidating Concrete (SCC) and sustainable Portland Cement replacements
- Extensive use of Excel's spreadsheet and database tools for data comparisons

WORK EXPERIENCE

Staff Engineer Intern – BL Companies (Land Development Design Firm) — **January 2022 – Present**
Harrisburg Office - Harrisburg, PA

- Assist in street and landscape design by utilizing AutoCAD Civil 3D
- Stormwater design calculations using TR-55 and EPANET program

Teaching and Lab Assistant – Civil Engineering Materials Laboratory — **August 2021 – December 2021**
Civil Engineering Department – Penn State Harrisburg, Middletown, PA

- Assist the lab investigation of physical and mechanical properties of civil engineering materials: soils, aggregates, concrete, steel; wood; and polymers
- Consulting the ASTM standards in guiding 30+ students/semester with lab tasks
- Lab materials and equipment preparation and grading lab reports

Civil Engineering Internship – Codes and Zoning **May 2021 – August 2021**

Middletown Borough Codes and Zoning Department, Middletown, PA

- Conducting the town's property maintenance & building codes inspection daily
- Consulting the county's GIS & Permit-Manager in managing the town's codes
- Inspecting Concrete Contractor's work for sidewalks and driveways around town

Global Ambassadors Student Coordinator and Office Worker **April 2019 - Present**

International Student Office – Penn State Harrisburg, Middletown, PA

- Facilitated students from +15 countries to develop leadership skills through team-building workshops and cultural events publicly attended by +300 people
- Documentation and organization of events, programs, surveys, and student data
- Collaborated with 3 different campuses to create a global leadership conference

PRESENTATION

"A Comparison Study and Optimization of Input Parameters for Thermal Conductivity Testing of Concrete" Paper presented *Drawdown Project*, University Park, PA. July 29th, 2021.

"Evaluation of Self-Consolidating Concrete Mixtures used with Mineral and Chemical Admixtures." Paper presented *at the Pennsylvania State University Virtual Multi-Campus Research Experience for Undergraduates (MC-REU)*, University Park, PA. July 26th, 2020.

SKILLS

Languages: English (professional fluency), Indonesian (native), Russian, and Malay (conversational)
Programs: Civil 3D, AutoCAD, ArcGIS, SolidWorks, MATLAB, Permit Manager, and Microsoft Office Suite

LEADERSHIP EXPERIENCE

American Society of Civil Engineers (ASCE), *Vice President* – Penn State Harrisburg **August 2018 - Present**

- Organize a close-knitted community of 30+ civil engineering students on campus
- Coordinate with local professional engineers to connect with students in meetings

Concrete Canoe Team – ASCE, *Co-Chair* – Penn State Harrisburg **July 2021 - Present**

- Support members in material preparations for concrete canoe competition in labs
- Organize team meetings and training in familiarizing with concrete works

Alternative Spring Break: San Diego, CA, *School Delegation* – Penn State Harrisburg **March 2020**

- Field studied the social and cultural impact of the US-Mexico border wall infrastructure and the gentrification of San Diego towards the Chicanos community
- Studied the history and cultural significance of the Chicanos community in San Diego through crafted murals on the side and under the interstate highways
- Worked on a mural restoration in a local community center with peer volunteers

International Service Center (ISC), ***volunteer*** – Harrisburg, PA **November 2021 - Present**

- Assist the ISC office in the Afghan refugee resettlement project in Central PA
- ISC representative to raise awareness of the Afghan Refugee crisis on campus
- Raised $500 in charity in addition of 5 boxes of supplies for donations to refugee
- Driving multiple trips to assist ISC in the arrival process of refugees in local airport

Engineering Without Borders (EWB), ***Member*** – Penn State Harrisburg **August 2018 – May 2019**

- Participate in local volunteering opportunities with fellow engineering peers

Tau Beta Pi National Engineering Honor Society, ***Member*** – Penn State **August 2020 – May 2021**

- Connecting with fellow impactful engineering students throughout the university

Global Ambassadors Program, ***Student Ambassador*** – Penn State Harrisburg **January 2019 – Present**

- Liaisons for the faculty of the school of Science, Engineering & Technology in facing cultural barriers in order to facilitate the integration of international students into the campus community

American Field Service (AFS), ***Int'l Community Volunteer*** **-** Indonesia, Russia, USA **July 2016 - Present**

- A year intercultural exchange program with AFS in a local Russian high school to exchange culture and languages between Russian and Indonesian communities
- Directed an orientation for 12 exchange students to 3 countries
- Assisted in teaching English for elementary school students in Russia
- Judge for US student candidates for the Speedwell Exchange Scholarship

Muslim Student Association, ***President*** – Penn State Harrisburg **July 2021 - Present**

- Coordinate with members in creating inclusive spaces for the Muslim minority
- Organizing the only weekly Friday prayers for the Muslim community on campus
- Empowering Muslim students with leadership and engagement opportunities

Berlayar Mentorship Project, ***Co-Founder and Mentor*** – Indonesia **July 2020 – November 2020**

- Co-founded and co-lead a mentorship project focusing on developing 25 local senior high-school students from a diverse

social-economic backgrounds in preparing themselves for the transition to college and the professional world

International Affairs Club/Rotaract, *School Delegation* – Penn State Harrisburg **August 2018 - Present**

- University delegation for Harvard Model United Nations in Boston, MA and the National Model United Nations in Washington D.C.
- Raised awareness in international affairs issues on campus and networking opportunities under Rotary International
- Committee chair for the Third Committee of the General Assembly (Social, Humanitarian & Cultural) in Penn State Harrisburg Model United Nations